Direct Flux Control of PM Synchronous Motor Drives for Traction Applications

Gianmario Pellegrino
Politecnico di Torino
gianmario.pellegrino@polito.it

Barbara Boazzo
Politecnico di Torino
barbara.boazzo@polito.it

Thomas M. Jahns
University of Wisconsin – Madison
jahns@engr.wisc.edu

***Abstract*- Three Permanent Magnet traction motors are controlled via a unified Direct Flux Vector Control scheme. Two of the motors have the same stator with concentrated windings, one combined with a Surface Mounted PM rotor and the other with an Interior PM rotor. The third motor is a PM-assisted Synchronous Reluctance motor with distributed windings. The algorithm has a predictive nature and no regulators that need to be tuned. When switching from one motor to another, the set of motor parameters is changed and nothing else. The key parameters are the stator resistance and the *dq* flux linkage curves. Drive commissioning issues are addressed along with the effects of parameter errors on the control performance, and both are quite acceptable for traction applications. Experimental results are provided for all three motors.**

***Index Terms*: Direct Flux Vector Control, Direct Torque Control, Permanent Magnet Machines, Permanent Magnet Motor Drives, Predictive Control, Deadbeat Control.**

I. INTRODUCTION

Battery electric and hybrid electric vehicles very often adopt Permanent Magnet (PM) traction motors for their powertrains [1-2]. Different PM motor topologies are in use, having different pros and cons. Concentrated-winding (CW) machines are appreciated by vehicle manufacturers for their assembly advantages and their compactness [3]. Other competitors prefer distributed windings and salient rotor structures [4-5] for their better transient overload power with a given inverter size and their larger high-efficiency operating regions within the boundaries of their torque-vs-speed capability curves.

When dealing with the control of an electric drive for traction applications, some key performance objectives can be identified, regardless of the PM motor type:

- Maximum exploitation of the inverter current and voltage limits over a large flux-weakening speed range;
- High robustness of the control against parameter uncertainties and variations of the operating temperature;
- Optimization of the motor efficiency at all speeds and, in particular, at partial loads.

Similar to Direct Torque Control (DTC), the Direct Flux Vector Control (DFVC) directly controls the flux linkage vector amplitude and phase angle to control the electromagnetic torque. DFVC adopts Space Vector Modulation at constant switching frequency for its PWM algorithm and uses a rotor position sensor, which is typical for traction applications. In previous work, DFVC has been applied to a wide range of sinusoidal AC motors including Induction and Synchronous Reluctance motors, as well as Interior and Surface PM (IPM and SPM) motors [6]. This controller has demonstrated its ability to exploit the inverter voltage and current limits very easily in the flux weakening speed region, and adapts easily to variable dc-link levels. At very high speeds, the Maximum Torque Per Voltage region (MTPV) is also exploited with relative ease.

Recently, a predictive version of the DFVC algorithm has been proposed and tested on a PM-assisted Synchronous Reluctance (SyR) motor, making it possible to reduce the calibration burden associated with the three PI regulators of the torque controller [7]. The predictive algorithm results in a more complicated flux observer scheme and requires a commissioning stage for the motor and the inverter. In return, the algorithm is applicable to any PM synchronous drive with no modification or tuning, making it very appealing for industrial applications. The simplification of the motor commissioning is another work in progress [15]. The objectives of this work are: 1) to provide experimental confirmation that predictive DFVC applies to different traction motors; and 2) to directly address the commissioning sequence and parameter sensitivity issues in order to demonstrate the feasibility of the proposed controller in production equipment.

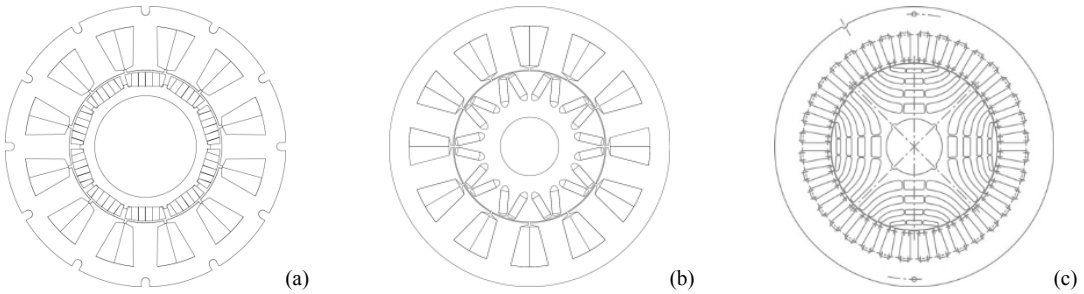

Fig. 1. Three types of PM traction motors tested during this investigation. Left) Surface Mounted PM with concentrated windings (CW-SPM); Center) Interior PM with Concentrated Windings (CW-IPM); Right) PM-assisted Synchronous Reluctance motor with distributed windings (PMASR).

II. PREDICTIVE DIRECT FLUX VECTOR CONTROL

The DFVC algorithm is based on the motor voltage model (1), expressed in the stator flux linkage reference frame (d_s,q_s) defined in Fig. 2. In (1), the control state variables λ and δ represent the flux linkage amplitude and the load angle, respectively. The d_s-axis direct voltage component is responsible for the flux amplitude closed-loop control, while the q_s-axis quadrature voltage controls the load angle δ, defined in Fig. 2 as the angle between the stator flux linkage and rotor d-axes.

$$\begin{cases} v_{ds} = R_s \cdot i_{ds} + \frac{d\lambda}{dt} \\ v_{qs} = R_s \cdot i_{qs} + \left(\frac{d\delta}{dt} + \omega\right) \cdot \lambda \end{cases} \quad (1)$$

Although the control is implemented in (ds,qs) coordinates, the magnetic model, also called the current model, is still conveniently expressed in the rotor synchronous reference frame (d,q):

$$\begin{cases} \lambda_d = L_d(i_d, i_q) \cdot i_d + \lambda_m \\ \lambda_q = L_q(i_d, i_q) \cdot i_q \end{cases} \quad (2)$$

The direct and cross-dependences of the inductances on the current components are evident in (2). Cross saturation is not expressed via explicit L_{dq} and L_{qd} terms, but its effects are implicitly taken into account in the form of L_d and L_q variations with i_d and i_q. When the two state variables λ and δ are directly used to express the torque, the non-linear expression is:

$$T = \frac{3}{2} p \left(\frac{\lambda \lambda_m}{L_d} \sin(\delta) - \frac{\lambda^2}{2L_q} \left(\frac{L_q}{L_d} - 1 \right) \sin(2\delta) \right) \quad (3)$$

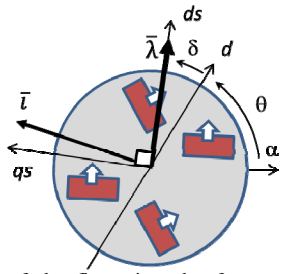

Fig. 2. Definition of the flux-oriented reference frame (ds, qs) for a generic PM motor rotor.

More conveniently for control purposes, the torque control algorithm relies on the λ - i_{qs} alternative expression (4), where i_{qs} is the current component in quadrature with the flux linkage vector:

$$T = \frac{3}{2} p \cdot \lambda \cdot i_{qs} \quad (4)$$

A. Predictive Direct Flux Vector Control Scheme

A block diagram of the DFVC algorithm is presented in Fig. 3. The construction of the λ and i_{qs} reference values from the torque reference comes from (4). The maximum current and voltage limits are included in the convenient form of ***two saturation blocks***: the saturation of i_{qs} bounds the current amplitude within the inverter limit, while the saturation of the flux linkage amplitude consistent with the motor speed and dc bus voltage insures that the steady-state motor voltage will remain within the limits of the inverter maximum voltage [6]. This is a very straightforward way to handle the flux weakening speed region since it is parameter-independent, making it insensitive to the motor in use.

The key block of the proposed control scheme is the one indicated as "Inverse Machine Model" in the figure, summarized by equation (6) presented hereafter. Such key equation expresses the load angle error as a function of the quadrature current and flux amplitude control errors.

B. Mathematical Derivation of the Load Angle Equation

The dq magnetic model (2) is reported to the stator field oriented frame (d_s,q_s) by a rotation by δ:

$$\begin{cases} \lambda = L_{ds} \cdot i_{ds} + L_{dqs} \cdot i_{qs} + \lambda_m \cos(\delta) \\ 0 = L_{dqs} \cdot i_{ds} + L_{qs} \cdot i_{qs} - \lambda_m \sin(\delta) \end{cases} \quad (5)$$

The inductance terms L_{ds}, L_{ds} and L_{dqs} in the new reference frame depend on L_d and L_q and on the load angle δ:

$$\begin{bmatrix} L_{ds} & L_{dqs} \\ L_{dqs} & L_{qs} \end{bmatrix} = \begin{bmatrix} L_0 - \Delta L \cos(2\delta) & \Delta L \sin(2\delta) \\ \Delta L \sin(2\delta) & L_0 + \Delta L \cos(2\delta) \end{bmatrix} \quad (6)$$

$$L_0 = \frac{L_d + L_q}{2} \qquad \Delta L = \frac{L_q - L_d}{2} \quad (7)$$

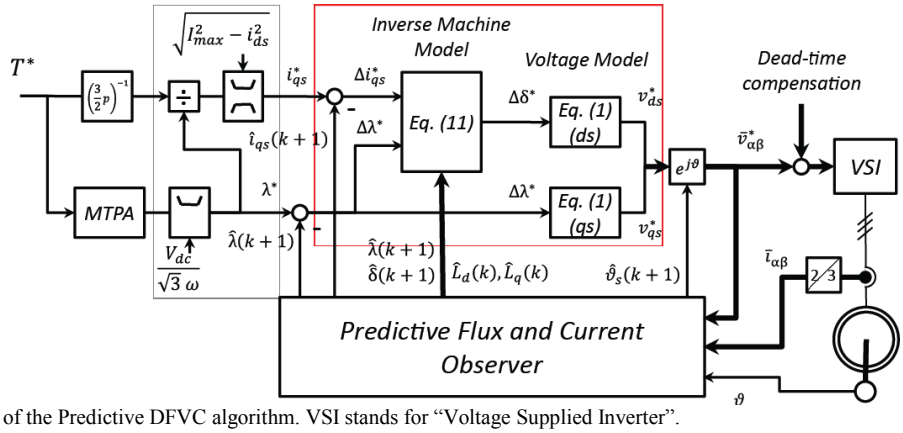

Fig. 3. Block diagram of the Predictive DFVC algorithm. VSI stands for "Voltage Supplied Inverter".

The magnetic equations (5) and (6) are now manipulated to find the relationship between the control errors $\Delta\lambda$ and Δi_{qs} and the corresponding load angle variation $\Delta\delta$. By differentiation of the two components of (5) equations (8a) and (9a) are found, the former referring to the d_s component of (5), and the latter to the q_s component.

$$\frac{di_{ds}}{dt} = \mathrm{A}\cdot\frac{d\lambda}{dt} + \mathrm{B}\cdot\frac{di_{qs}}{dt} + \mathrm{C}\cdot\frac{d\delta}{dt} \tag{8a}$$

$$\begin{cases} \mathrm{A} = \dfrac{1}{L_0 - \Delta L\cos(2\delta)} \\ \mathrm{B} = -\dfrac{\Delta L\sin(2\delta)}{L_0 - \Delta L\cos(2\delta)} \\ \mathrm{C} = -\dfrac{2\Delta L\left(\sin(2\delta)i_{ds} + \cos(2\delta)i_{qs}\right) - \lambda_m\sin(\delta)}{L_0 - \Delta L\cos(2\delta)} \end{cases} \tag{8b}$$

$$\frac{di_{ds}}{dt} = \mathrm{B}'\cdot\frac{di_{qs}}{dt} + \mathrm{C}'\cdot\frac{d\delta}{dt} \tag{9a}$$

$$\begin{cases} \mathrm{B}' = -\dfrac{L_0 + \Delta L\cos(2\delta)}{\Delta L\sin(2\delta)} \\ \mathrm{C}' = -\dfrac{2\Delta L\left(\cos(2\delta)i_{ds} - \sin(2\delta)i_{qs}\right) - \lambda_m\cos(\delta)}{\Delta L\sin(2\delta)} \end{cases} \tag{9b}$$

The time derivative of i_{ds} is put in evidence in (8a) and (9a), so that it can be eliminated by equaling the respective right-hand sides of the two equations. The time derivatives remeaining in the final equation (10) after the simplification of di_{ds}/dt are the ones of λ, i_{qs} and δ.

$$(\mathrm{C} - \mathrm{C}')\cdot\frac{d\delta}{dt} = (\mathrm{B}' - \mathrm{B})\cdot\frac{di_{qs}}{dt} - \mathrm{A}\cdot\frac{d\lambda}{dt} \tag{10}$$

A further manipulation leads to the expression of the load angle variation in the discrete-time domain:

$$\Delta\delta^* = \frac{\Delta i_{qs}^* + \frac{[\hat{\xi}(k)-1]}{2\hat{L}_q(k)}\cdot\Delta\lambda^*}{\frac{\cos[\hat{\delta}(k+1)]}{\hat{L}_d(k)}\cdot\lambda_m - \frac{[\hat{\xi}(k)-1]\cdot\cos[2\hat{\delta}(k+1)]}{\hat{L}_q(k)}\cdot\hat{\lambda}(k+1)} \tag{11}$$

As anticipated, the load angle variation (11) is a function of the two control errors $\Delta\lambda^*$ and Δi_{qs}^*. Moreover, it is also a function of the magnetic model parameters L_d, L_q, λ_m and of the predicted magnitude and phase of the flux linkage vector (λ, δ). All those variables are generated by the ***Predictive Flux and Current Observer*** block, that is the key block of the proposed control scheme.

C. Predictive Flux and Current Observer

The "predictive" nature of the observer refers to the fact that some of the observed quantities are evaluated at the next actuation instance ($k+1$) in a predictive fashion, where (k) represents the current computational time instant of the real-time digital controller [8-9]. The prediction at time ($k+1$) is critically important in model-based controllers for compensating the actuation delay of the digital controller. Without it, the control response is nervous and oscillatory [10-11].

The discrete-time block scheme of the predictive observer is represented in Fig. 4. The input stage is a closed-loop, non-predictive stator flux observer, where the current-to-flux model in (d,q) coordinates serves the low-speed operating region, and the voltage model in (α,β) coordinates serves the higher-speed range [6,11]. The crossover angular frequency between the low- and high-speed models is set by the observer feedback gain g (electrical rad/s). The control reference voltage signals are used as the observer inputs instead of voltage measurements and the rotor position comes from an encoder. The output of the first observer stage is the flux linkage vector in (d,q) coordinates, referred to the current time instant (k). From this flux linkage estimate, the (d,q) inductances are evaluated according to (6) for use in predicting the current and the flux linkage at time step ($k+1$):

$$\begin{cases} \hat{L}_d(k) = \dfrac{\hat{\lambda}_d(k) - \lambda_m}{i_d(k)} \\ \hat{L}_q(k) = \dfrac{\hat{\lambda}_q(k)}{i_q(k)} \end{cases} \tag{6}$$

The (d,q) current components are predicted at time ($k+1$) by means of discrete-time integration based on (7):

$$\begin{cases} L_d\,\dfrac{di_d}{dt} = v_d - R_s i_d + \omega\lambda_q \\ L_q\,\dfrac{di_q}{dt} = v_q - R_s i_q - \omega\lambda_d \end{cases} \tag{7}$$

Finally, the (d,q) flux linkage at time ($k+1$) are calculated from the newly-calculated current components by means of (2). The amplitude and phase angle (δ, θ_s) of the flux linkage vector in the various reference frames are finally calculated using simple mathematics that is not represented in the figure.

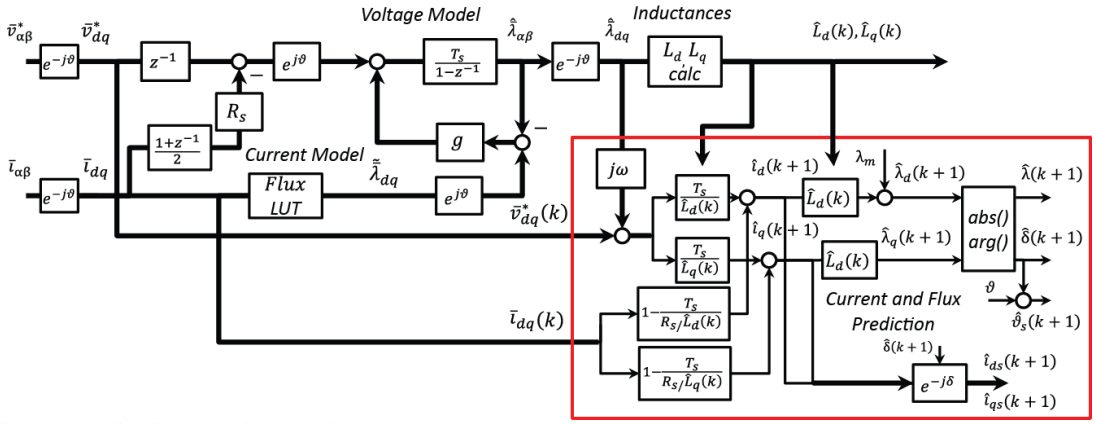

Fig. 4. Predictive stator flux linkage and current observer.

D. Commissioning of the Inverter and of the Motor

The apparently complicated algorithm summarized by the block diagrams in Figs. 3 and 4 has the appealing feature of segregating its dependencies on the motor and inverter parameters into a very limited set of blocks. The motor parameters to be changed when switching to a new motor are the *stator* ***resistance*** R_s (Fig. 4), the ***Current to Flux Linkage Look Up Tables*** (Flux LUT in Fig. 4) and the ***PM flux linkage*** λ_m, again in Fig. 4, on the right side. The inverter parameters are included in the "Dead-Time Compensation" term in Fig. 3.

With no tuning required for the DFVC algorithm except for these parameters, the commissioning of the inverter and the motor is critical for this control. The inverter self-identification and compensation technique described in [12] is used here, which includes also the identification of the initial motor resistance. Other techniques from the literature are also effective.

The motor magnetic model is identified via the off-line procedure described in [13], where the flux linkage curves are evaluated with the motor driven at constant speed by a speed-controlled dynamometer machine. The literature proposes other techniques for the identification of the motor model, and a comprehensive self-identification method has been recently proposed [15].

E. Parameters Detuning

The detuning of the two parameters R_s and λ_m due to temperature effects is not particularly critical. The former introduces an error in the voltage-model based flux estimate (Fig. 4), whose effect would be consistent only at low speed where it is the current model that mostly contribute to the flux estimate. Plus, R_s can also introduce a small voltage actuation error (Fig. 3), that is negligible in most of cases also for large temperature variations (100°C of temperature rise mean +40% the resistance). In case of critical applications a technique for the on-line estimation of the stator resistance can be integrated into the proposed control [16]. Dealing with the PM flux linkage λ_m the effect of its detuning produces a torque scale error, as addressed in section III. Also in this case, critical applications can require the use of existing method for on-line parameter adaptation [17].

Once the motor model is identified and the dead-time effect is compensated, the observer gain g is not particularly critical. Typical values are 200 to 600 rad/s for an inverter switching frequency of 8 kHz, with almost no sensitivity to the controlled motor. Other than the commissioning stage and the observer gain, there are no additional adjustments required for the described control algorithm.

F. Motor Efficiency

The optimization of the steady-state motor efficiency is straightforward with DFVC. Motor losses can be roughly divided into load-dependent and speed-dependent losses. The load-dependent losses are mainly copper losses and vary with the square of the current amplitude, while the speed-dependent losses depend on the flux linkage amplitude. Harmonic loss is an additional speed-dependant loss, but its minimization is more related to the machine design, rather than to the adopted control technique. Copper loss are minimum along the Maximum Torque Per Ampere (MTPA) trajectory, whereas iron losses are mimimum along the MTPV one, which is normally utilized only at high speed. The control scheme of Fig. 3 uses the MTPA below the corner speed: in this way, the major low speed loss component (copper loss) is inherently minimized. When the voltage limit is reached, the flux is weakened and the q_s current component adapted to maintain the torque setpoint, where possible. In this way, the operating point drifts gradually from the MTPA to the MTPV with the speed increase, and this is compatible with a maximum efficiency strategy. A more accurate, machine custom maximization of the efficiency requires further identification of the specific motor, and additional blocks including custom built look up tables or custom loss models. These additional features can be integrated into the proposed scheme, but are out of the scope of this paper.

III. Experimental Results

A. Experimental Setup and Machine Prototypes

The experiments have been run on two different test rigs, both equipped with dSPACE Controller boards. Fig. 5 reports the one used for the IPM and SPM machines. The machine under test is in the square at the bottom right corner, connected to an induction machine dyno via a torque-meter (not visible). The power converters are in the other square on the left hand corner. The setup used for the PM-SyR machine is similar to all extents.

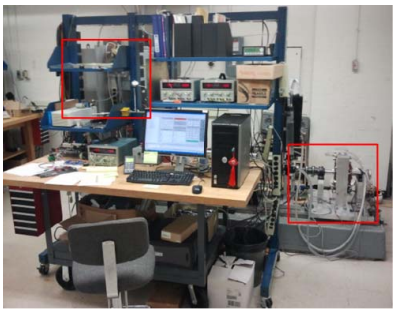

Fig. 5. Experimental setup used for the IPM and the SPM machines.

The cross-sections of the three tested motors are illustrated in Fig. 1, and teir ratings are in Table I. The CW-IPM and SPM machines [14] are rated to deliver 30 kW (cont.) at 14,000 rpm maximum speed, in accordance with the specifications of the FreedomCar 2020 machine. They have a common stator and replaceable rotors. The rotor switch operation is documented in Fig. 6ab. The ends of the concentrated windings and the pipes for liquid cooling are also visible in the figures. The PM-assisted SyR motor is the one used in [7], a 7 kW, 10,000 rpm maximum speed machine designed for an electric scooter.


(a)


(b)


(c)

Fig. 6. Switching from the IPM (a) to the SPM (b) rotor for the concentrated-winding motors of [14]. (c) Rotor of the PM-assisted Synchronous Reluctance motor used in [7].

B. Torque Step Response

The results in Fig. 7 demonstrate the fast and non-oscillatory torque step response delivered by the predictive DFVC algorithm for the 3 motors. In Figs. 7a) and 7b), the response to a 30 Nm step is shown for the SPM and the IPM motors, respectively. The speed is controlled at 100 rpm by the dyno machine, representative of the low-speed region where the flux linkage is estimated via the current model. The estimated torque, the duty cycles and the phase currents plots are shown. The slower rate of change of the IPM motor torque with respect to the SPM machine is due to its higher inductance value. That is, the IPM flux linkage has to vary by larger amount for the same 30 Nm target torque, so the time interval with saturated duty-cycles is longer in Fig. 7b than in Fig. 7a, reflecting the higher value of Volt-sec needed by the high-inductance IPM motor.

Fig. 7c shows the response of the PM-assisted SyR machine to ± 5 Nm torque step reversals at no-load. The speed varies between ±2000 rpm and the torque step reversals occur at maximum speed.

C. Detuning Effects

Two examples of parameter detuning effects are illustrated in Fig. 8 for the CW-IPM motor. If dead-time errors are not properly compensated (Fig. 8a) erratic oscillations of the duty-cycles are visible during steady-state operation, leading to noise, vibration, and additional losses. The impact of PM temperature variations is illustrated in Fig. 8b. The motor under test is driven at constant speed (100 rpm) by the dyno at room temperature (24°C). The 30 Nm torque step test of Fig. 7b is repeated here three times. The first test (blue traces) is with no parameter detuning. In the second test (green traces), the PM flux linkage is purposely overestimated by 10% in the DFVC software to emulate the effect of a PM temperature increase. The +10% flux linkage difference corresponds to a temperature increase of 50°C for a total of 74°C, given the -0.2%/°C thermal variation coefficient of Nd PMs. In a similar manner, the red traces refer to a PM flux linkage overestimate of +20%, or an emulated temperature increase of +100°C, for a total of 124°C. The test results confirm that the control response is insensitive to the detuning in terms of stability. The "detuned" tests deliver reduced torque with respect to the 30 Nm set-point even though the estimated torque indicates 30 Nm in all three cases. The torque reduction is visible in the (i_d, i_q) graph of Fig. 8b, basically in the smaller iq component of the detuned tests. The final torque values are: 30 Nm (24°C), 28 Nm (74°C) and 26 Nm (124°C).

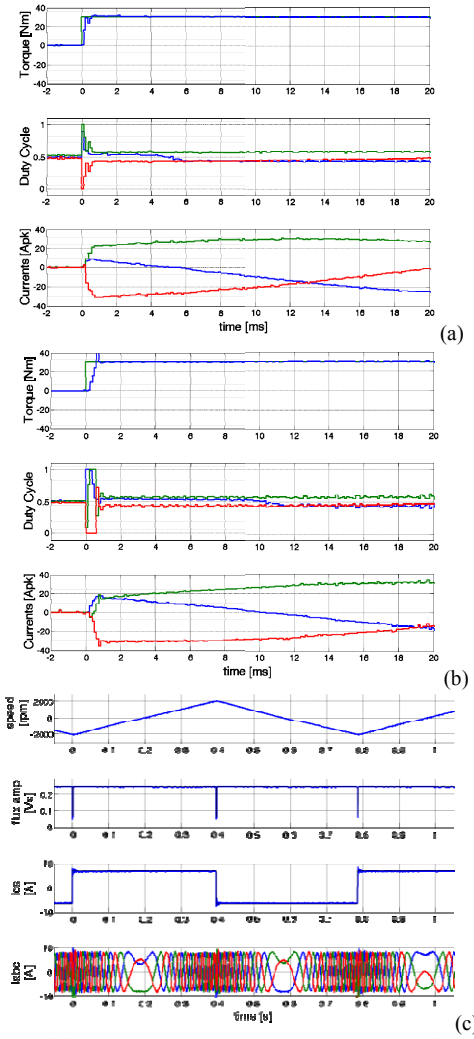

Fig. 7. a) and b) 0 - 30 Nm step response at 100 rpm. (a) is the CW-SPM motor, (b) is the CW-IPM motor. Top: estimated torque [Nm], Center: phase duty-cycles; Bottom: phase currents [A]. c) 5 Nm torque reversals of the PM-SyR at no load. Top to bottom: speed [rpm], observed flux amplitude [Vs], *qs*-current component [A], phase currents [A].

IV. Conclusion

This work has succeeded in demonstrating the promising characteristics of the Direct Flux Vector Control algorithm for PM synchronous machines intended for industrial and traction applications. The predictive version of the DFVC algorithm has been implemented and successfully tested with three different types of PM machines during this

investigation. The results from these tests confirm both the desirable dynamic response that is achieved using DFVC algorithm, as well as the high level of parameter insensitivity that the predictive version of the DFVC algorithm is capable of delivering. However, the predictive DFVC algorithm still requires information about the key PM machine parameters even though they are segregated into only a couple blocks in the controller. This requires a robust drive commissioning process to identify the values of these parameters when the PM motor is first connected, as well as continued tuning of the parameters during operation in order to compensate for the effects of temperature changes. Work is continuing to investigate improvements of the DFVC algorithm for PM machines in order to improve its performance and parameter insensitivity characteristics in order to enhance its suitability for demanding applications including traction drives.

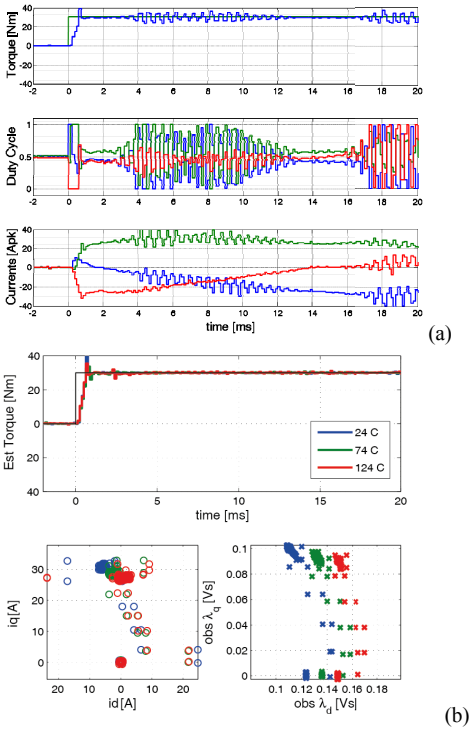

Fig. 8. Parameter detuning. a) Same test as in Fig. 7b), without dead-time compensation; b) Effect of overestimating the PM flux linkage parameter by 10% and 20%, corresponding to the values at 74°C and 124°C, respectively.

TABLE I. MAIN RATINGS OF THE THREE MACHINES UNDER COMPARISON

	IPM	SPM	PM-SyR
Number of slots	12		36
Pole pairs (p)	5		2
Stator outer diameter	274		150
Stack length [mm]	73.4		142
Airgap [mm]	0.73	1.85	0.3
Rated speed [rpm]	2800		2450
Rated Torque [Nm]	102		27
Rated current [Apk]	113	109	28
Characteristic current [Apk]	50	87	14
Dc-link voltage [V]	320	320	400
Open-circuit voltage line to line [Vpk]	314	328	60
Inertia [kg m^2]	$21 \cdot 10^{-3}$	$21 \cdot 10^{-3}$	$4.3 \cdot 10^{-3}$
Type of cooling	liquid		natural ventilation

REFERENCES

[1] Burress, T.; Campbell, S., "Benchmarking EV and HEV power electronics and electric machines", Transportation Electrification Conference and Expo (ITEC), 2013 IEEE , pp.1,6, 16-19 June 2013.

[2] Zhu, Z.Q.; Howe, D.; "Electrical Machines and Drives for Electric, Hybrid, and Fuel Cell Vehicles," Proceedings of the IEEE, vol.95, no.4, pp.746-765, April 2007.

[3] EL-Refaie, A.M., "Fractional-Slot Concentrated-Windings Synchronous Permanent Magnet Machines: Opportunities and Challenges," Industrial Electronics, IEEE Transactions on , vol.57, no.1, pp.107,121, Jan. 2010

[4] Rahman, K.; Jurkovic, S.; Stancu, C.; Morgante, J.; Savagian, P., "Design and performance of electrical propulsion system of extended range electric vehicle (EREV) Chevrolet Voltec," Energy Conversion Congress & Expo (ECCE), 2012 IEEE , pp. 4152-4159, Sept. 2012

[5] T. A. Burress, S. L. Campbell, C. L. Coomer, C. W. Ayers, A. A. Wereszczak, J. P. Cunningham, L. D. Marlino, L. E. Seiber, H. T. Lin, "Evaluation of the 2010 Toyota Prius Hybrid Synergy Drive System", ORNL/TM-2010/253(2010)

[6] Pellegrino, G.; Bojoi, R.I.; Guglielmi, P.; , "Unified Direct-Flux Vector Control for AC Motor Drives," Industry Applications, IEEE Transactions on , vol.47, no.5, pp.2093-2102, Sept.-Oct. 2011

[7] Boazzo, B.; Pellegrino, G., "Predictive direct flux vector control of Permanent Magnet Synchronous Motor drives," Energy Conversion Congress and Exposition (ECCE), 2013 IEEE , vol., no., pp. 2086-2093, 15-19 Sept. 2013.

[8] Maes, J.; Melkebeek, J., "Discrete time direct torque control of induction motors using back-EMF measurement," Industry Applications Conference, 1998. Thirty-Third IAS Annual Meeting. The 1998 IEEE , vol.1, no., pp.407-414 vol.1, 12-15 Oct. 1998

[9] Kenny, B.H.; Lorenz, R.D.; , "Stator- and rotor-flux-based deadbeat direct torque control of induction machines," Industry Applications, IEEE Transactions on , vol.39, no.4, pp. 1093- 1101, July-Aug. 2003

[10] Lee, J. S.; Choi, C. H.; Seok J.K.; Lorenz, R.D, "Deadbeat-Direct Torque and Flux Control of Interior Permanent Magnet Synchronous Machines With Discrete Time Stator Current and Stator Flux Linkage Observer," Industry Applications, IEEE Transactions on, vol.47, no.4, pp.1749-1758, July-Aug. 2011.

[11] Jensen, P. L. and Lorenz, R. D., "A physically insightful approach to the design and accuracy assessment of flux observers for field oriented induction machine drives", IEEE Trans. Ind. Appl., vol. 30, no. 1, pp. 101 -110, 1994.

[12] Pellegrino, G.; Bojoi, R.I.; Guglielmi, P.; Cupertino, F., "Accurate Inverter Error Compensation and Related Self-Commissioning Scheme in Sensorless Induction Motor Drives," Industry Applications, IEEE Transactions on , vol.46, no.5, pp.1970,1978, Sept.-Oct. 2010

[13] Armando, E.; Bojoi, R.I.; Guglielmi, P.; Pellegrino, G.; Pastorelli, M., "Experimental Identification of the Magnetic Model of Synchronous Machines," Industry Applications, IEEE Transactions on , vol.49, no.5, pp.2116,2125, Sept.-Oct. 2013

[14] Reddy, P.B.; EL-Refaie, A.M.; Kum-Kang Huh; Tangudu, J.K.; Jahns, T.M., "Comparison of Interior and Surface PM Machines Equipped With Fractional-Slot Concentrated Windings for Hybrid Traction Applications," Energy Conversion, IEEE Transactions on , vol.27, no.3, pp.593,602, Sept. 2012

[15] Pellegrino, G.; Boazzo, B.; Jahns, T.M.; "Magnetic Model Self-Identification for PM Synchronous Machine Drives", International Conference on optimization of electrical and electronic equipment (OPTIM) 2014, May 2014, accepted for presentation.

[16] Piippo, A.; Hinkkanen, M.; Luomi, J., "Adaptation of Motor Parameters in Sensorless PMSM Drives," Industry Applications, IEEE Transactions on , vol.45, no.1, pp.203,212, Jan.-feb. 2009

[17] Xi Xiao; Changming Chen; Meng Zhang, "Dynamic Permanent Magnet Flux Estimation of Permanent Magnet Synchronous Machines," Applied Superconductivity, IEEE Transactions on , vol.20, no.3, pp.1085,1088, June 2010